Smart Structures and Systems, *Vol. 17, No. 4 (2016) 631-646*
DOI: http://dx.doi.org/10.12989/sss.2016.17.4.631

Operation of battery-less and wireless sensor using magnetic resonance based wireless power transfer through concrete

Ji-Min Kim[1a], Minseok Han[2b], Hyung Jin Lim[1c], Suyoung Yang[1d] and Hoon Sohn[*1]

[1]*Department of Civil Engineering, Korean Advanced Institute for Science and Technology, 291 Daehak-ro, Yuseong-gu, Daejeon 34141, Republic of Korea*
[2]*Electronics Department, Osan University, 45 Cheonghak-ro, Osan, 18119, Republic of Korea*

(Received December 22, 2015, Revised February 20, 2016, Accepted February 26, 2016)

Abstract. Although the deployment of wireless sensors for structural sensing and monitoring is becoming popular, supplying power to these sensors remains as a daunting task. To address this issue, there have been large volume of ongoing energy harvesting studies that aimed to find a way to scavenge energy from surrounding ambient energy sources such as vibration, light and heat. In this study, a magnetic resonance based wireless power transfer (MR-WPT) system is proposed so that sensors inside a concrete structure can be wirelessly powered by an external power source. MR-WPT system offers need-based active power transfer using an external power source, and allows wireless power transfer through 300-mm thick reinforced concrete with 21.34% and 17.29% transfer efficiency at distances of 450 mm and 500 mm, respectively. Because enough power to operate a typical wireless sensor can be instantaneously transferred using the proposed MR-WPT system, no additional energy storage devices such as rechargeable batteries or supercapacitors are required inside the wireless sensor, extending the expected life-span of the sensor.

Keywords: wireless power transfer; wireless sensor; magnetic resonance; steel-reinforced concrete; structural health monitoring

1. Introduction

The number of aging civil infrastructure systems is increasing worldwide, and catastrophic failures of these infrastructure systems are often reported in the media (Sohn *et al.* 2004, Farhey 2005, Hao 2010). Therefore, there is increasing need to continuously monitor the safety and structural integrity of these systems, and indeed, various structural health monitoring (SHM) systems have been proposed and successfully implemented in the field (Raghavan *et al.* 2007, Lopez-Higuera *et al.* 2011, Nguyen *et al.* 2015, Li *et al.* 2015, Schallhorn *et al.* 2015). In spite of these recent flourishing SHM activities, the costs associated with installation and maintenance of the SHM systems remain expensive (Lynch *et al.* 2006).

*Corresponding author, Professor, E-mail: sohnhoon@kaist.ac.kr
[a] Ph.D. Student, E-mail: jimin.kim@kaist.ac.kr
[b] Professor, E-mail: mshan1024@osan.ac.kr
[c] Ph.D., E-mail: limnice87@kaist.ac.kr
[d] Ph.D. Student, E-mail: suyoung091@kaist.ac.kr

 ISSN: 1738-1584 (Print), 1738-1991 (Online)

To ease the installation and cabling issues associated with SHM, wireless sensing using radio frequency (RF) technology has become popular (Lynch *et al.* 2006). Lynch *et al.* (2006) installed wireless accelerometers into Geumdang Bridge in South Korea, and validated the field performance of wireless monitoring system to investigate the bridge responses to 40 ton truck loading such as modal frequencies and their mode shapes by changing the speed of the truck. Jang *et al.* (2010) and Cho *et al.* (2010) deployed a total of 70 wireless accelerometers and anenometers at Jindo Bridge in South Korea, and proved its capability by making comparisons with the existing wired SHM system in the bridge. Hu *et al.* (2013) designed wireless sensor network including an acceleration sensor and a strain sensor to monitor an in-service Zhengdian Highway Bridge in Wuhan, China. Dynamic responses are measured under random and moving vehicle loadings, and the bridge's safety performance state is estimated using the analyzed dynamic displacement through the data acquisition of wireless sensor network.

Currently, solid-state battery is the most common power source for wireless sensor. However, the battery should be periodically replaced or recharged. The use of a battery also compromises the ruggedness of the wireless sensor, because moisture can penetrate through the battery interface and the effectiveness of the rechargeable battery deteriorates over time. In addition, energy harvesting techniques are being developed to harness energy from surrounding ambient energy sources such as vibration, (Jung *et al*. 2011), natural light (Alippi *et al*. 2008) and temperature gradients (Tan *et al*. 2011). However, the amount of energy that can be harnessed from these techniques are often limited, especially for sensors using actuation components.

Alternatively, wireless power transfer techniques using inductive coupling (Moon *et al.* 2014, Dai *et al.* 2015), RF (Visser *et al.* 2013), laser (Park *et al.* 2010) have been proposed. Though inductive coupling successfully transfers kW-level power with high power transfer efficiency (PTE) over 90 %, the transfer distance is still limited to a few centimeters. RF techniques succeed in extending the transfer distance to a few meters, but the transfer power and PTE are significantly reduced to a μW-level and less than 1%, respectively. With a laser technique, even though PTE is not affected by the transfer distance, there is a critical restriction in that power cannot be transferred if there is an obstacle between the transmitter and receiver.

Magnetic resonance is used to transfer a few Watts of power over tens of centimeters (Kurs *et al*. 2007, Sample *et al.* 2009, Imura and Hori 2011). The advantage of magnetic resonance techniques is that they can transfer power through various media, including concrete (Jonah and Georgakopoulos 2013). In Jonah's experiments, Φ-200 mm transmitting (Tx) and receiving (Rx) resonators at a resonant frequency of 39.37 MHz was used. Tx resonator was located 100 mm above the concrete surface; Rx resonator was embedded in the concrete reinforced with Φ-2.2 mm crossed rebar. PTE was measured by changing the embedded depth of Rx resonator from 100 mm to 500 mm in 100 mm increments. When the total distance between resonators was 300 mm and 400 mm, PTEs before rectification were 35% and 25%, respectively. Then, 1 W of rectified power was ultimately transferred to a receiver load of 50 Ω.

In this study, a magnetic resonance based wireless power transfer (MR-WPT) system is developed so that power can be transferred over steel-reinforced concrete, and a battery-less and wireless sensor for fatigue crack detection can be powered. The uniqueness of this study lies in the following: (1) the performance of MR-WPT system is evaluated against a steel-reinforced concrete structure fabricated using Φ-15 mm steel rebar and a mix-proportion of a typical bridge deck, (2) MR-WPT system is used for operating a battery-less and wireless sensor specially designed for fatigue crack detection, and (3) PTE over free space, plain concrete, and concrete with embedded steel rebar is investigated.

The paper is organized as follows. In Section 2, the working principle of MR-WPT system is explained with an equivalent circuit model, and the influences of concrete and steel rebar are described. In Section 3, the hardware design and components of MR-WPT system including a Class-E power amplifier, a voltage rectifier circuit and resonators are described. Performance of the developed MR-WPT system is experimentally validated by evaluating PTE through a steel-reinforced concrete in Section 4. A brief summary and future work are provided in Section 5.

2. Working principle of magnetic resonance based wireless power transfer (MR-WPT) system

Fig. 1 schematically shows the basic configuration of MR-WPT system. The system consists of a transmitting (Tx) resonator, a receiving (Rx) resonator, a primary circuit and a secondary circuit. The primary circuit is composed of a DC power source, a DC-AC inverter, a power amplifier and a matching network, and the secondary circuit includes a matching network, a full bridge rectifier, a DC-DC converter and a load (a wireless sensor).

The DC power source supplies power to the primary circuit, and the DC-AC inverter generates AC power. Then, the power amplifier intensifies the power level, and drives Tx resonator through the impedance matching network, which maximizes PTE and minimizes power reflected back to the primary circuit. Tx resonator generates alternating magnetic fields causing magnetic coupling with Rx resonator. MR-WPT system utilizes a resonance of magnetic field between Tx and Rx resonators as a link of power transfer. The resonant frequencies of Tx and Rx resonators are carefully matched so that they can be strongly coupled to each other with negligible radiation loss (Wei X *et al.* 2014, Sample *et al.* 2009, Imura and Hori 2011). The AC power transferred to Rx resonator is linked to the secondary circuit through another impedance matching network, and rectified to DC power through the full bridge rectifier. Finally, DC power is fed to the wireless sensor, after voltage conversion to the operating voltage of the wireless sensor.

An equivalent circuit model of MR-WPT system is shown in Fig. 2 (Beh *et al.* 2013). The primary circuit is modeled as an AC voltage source with an amplitude of *Vs* and a source impedance of Z_S, and the secondary circuit is represented by a load impedance of Z_L. The resonant frequency, *f*, of Tx and Rx resonators can be expressed as follows and tuned by adjusting equivalent lumped *L* and *C* values.

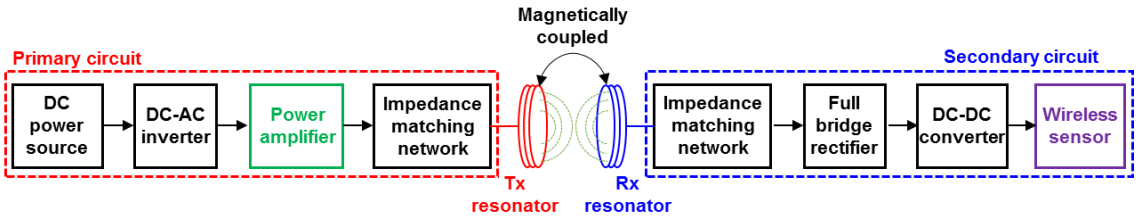

Fig. 1 Schematic diagram of the proposed MR-WPT system consisting of a Tx resonator, a Rx resonator, a primary circuit and a secondary circuit

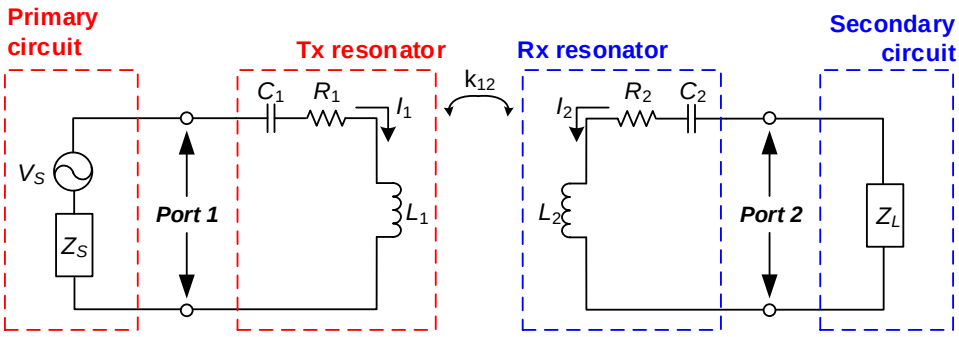

Fig. 2 Equivalent circuit model of MR-WPT system

$$f = 1/2\pi\sqrt{L_i C_i} \qquad (i = 1,\ 2) \tag{1}$$

$$Q_i = 2\pi f \cdot L_i / R_i \qquad (i = 1, \tag{2}$$

where L_i, C_i and R_i are respectively the inductance, capacitance and resistance of the ith resonator, and subscripts 1 and 2 denote Tx and Rx resonator, respectively. Q_i is a quality factor of the ith resonator, and this value highly affects PTE of MR-WPT system (Wei *et al.* 2014). The strength of the magnetic coupling between Tx and Rx resonators can be expressed by a coupling coefficient between them.

$$k_{12} = M_{12} / \sqrt{L_1 L_2} \tag{3}$$

where k_{12} is a coupling coefficient ranging between 0 and 1, and M_{12} is a mutual inductance induced by the magnetic coupling.

Viewed as a two-port network that transfers power from port 1 to port 2, as shown in Fig. 2, MR-WPT system can be evaluated using S-parameters: reflection and transmission coefficients, S_{11} and S_{21}. S_{11} denotes the ratio of the power reflected back to port 1, and S_{21} represents the ratio of the power transmitted to port 2 both with respect to the initial power at port 1. Therefore, smaller S_{11} and larger S_{21} represent a higher power transfer performance. S_{11} decreases as the impedances of the primary circuit and Tx resonator match. S_{21} relies on resonator properties such as k_{12}, Q_1 and Q_2.

PTE of MR-WPT system can be analytically estimated using the equivalent circuit model in Fig. 2 (Beh *et al.* 2013). Node equations for the equivalent circuit model can be expressed using Eqs. (4) and (5).

$$\begin{bmatrix} V_S \\ 0 \end{bmatrix} = \begin{bmatrix} Z_1 & j\omega M_{12} \\ j\omega M_{12} & Z_2 \end{bmatrix} \begin{bmatrix} I_1 \\ I_2 \end{bmatrix} \tag{4}$$

where

$$Z_1 = Z_S + R_1 + j\left(\omega L_1 - \frac{1}{\omega C_1}\right) \qquad Z_2 = Z_L + R_2 + j\left(\omega L_2 - \frac{1}{\omega C_2}\right) \tag{5}$$

Z_1 and Z_2 are the impedances at ports 1 and 2, respectively, and they are typically tuned to 50 Ω in practice. ω (=$2\pi f$) is an angular resonant frequency, and I_1 and I_2 are current flowing through Tx and Rx resonators, respectively. Transferred power to port 2 induces the following load voltage, V_L, computed from Eq. (6).

$$V_L = -I_2 \cdot Z_L = \left(\frac{V_S \cdot (j\omega M_{12})}{Z_1 Z_2 + \omega^2 M_{12}^2}\right) \cdot Z_L \tag{6}$$

Since V_S, ω and Z_L are the constant parameters of the system, V_L is determined by M_{12} that is directly related to the coupling coefficient, k_{12}. S_{21} can be calculated using Eq. (7) (Sample *et al.* 2009), and the final PTE of MR-WPT system is computed by squaring S_{21} in Eq. (8).

$$S_{21} = 2\frac{V_L}{V_S}\left(\frac{Z_S}{Z_L}\right)^{1/2} \tag{7}$$

$$\text{PTE} = |S_{21}|^2 \times 100\ (\%) \tag{8}$$

In this study, reinforced concrete consisting of a concrete slab reinforced with steel rebar is located between Tx and Rx resonators. Concrete is a lossy dielectric material with complex permittivity (Ogunsola *et al.* 2006), and steel rebar is a conductive and ferromagnetic material. Numerous studies have been conducted with respect to electro-magnetic (EM) losses due to concrete and reinforcement (Richalot *et al.* 2003, Antonini 2003). EM losses occur mainly by two mechanisms: reflection and absorption. (Roh *et al.* 2008). Fig. 3 describes EM wave losses in passing through reinforced concrete. A portion of the incident EM wave, I(t), is reflected at the entering surface of the concrete, $R_1(t)$.

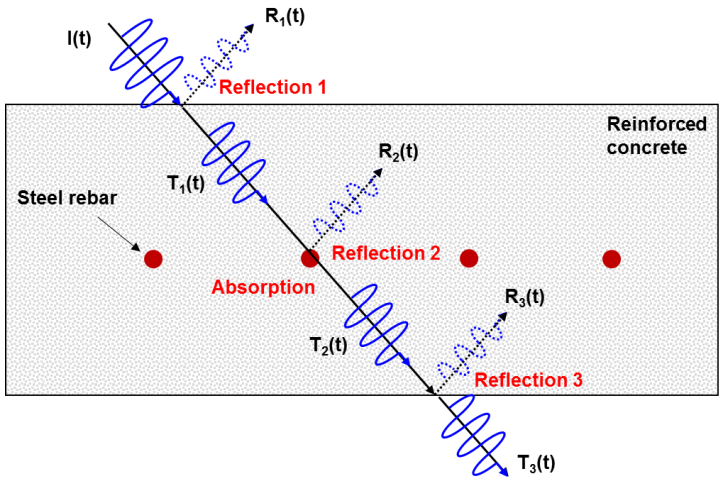

Fig. 3 Losses of the electro-magnetic waves propagating through a reinforced concrete structure

The transmitted EM wave, $T_1(t)$, continuously propagates, but undergoes attenuation through the concrete medium. Then, the secondary EM reflection loss, $R_2(t)$, occurs at the surface of steel rebar, as well as absorption loss that culminates with EM energy being transformed into thermal energy. Part of the remaining EM wave, $T_2(t)$, is reflected at the exiting surface of the concrete once again, (i.e., $R_3(t)$), and the subsequent transmitted EM wave, $T_3(t)$, is the actual EM wave transferred to Rx resonator.

3. Development of magnetic resonance based wireless power transfer (MR-WPT) system

Fig. 4 shows a spiral type resonator designed for this study. The resonance frequency of the resonator is 1.7 MHz, because of its tolerably-low sensitivity to surrounding ferromagnetic and dielectric materials. A 2.3 mm thick litz-wire is used to wind the resonator. The wire is turned 7 times, and the spacing between any two adjacent wires is 2.3 mm. The inner and outer diameters of the resonator are 270 mm and 330 mm, respectively. To stably keep its shape and strength, the front and back sides of the manufactured spiral type resonator are covered by a 420 × 420 × 3 mm^3 (H × W × T) acrylic plate with a Φ 220 mm hole at the center. The inductance and resistance of Tx and Rx resonators are 30.3 μH, 29.7 μH, 0.2 Ω and 0.2 Ω, respectively, and quality factor (Q) is more than 250 for both resonators.

The series (C_s) and shunt (C_p) chip capacitors in the additional frequency tuning board at the end of each resonator are adjusted to tune the resonant frequency and impedance of each resonator to 1.7 MHz and 50 Ω at the same time. Design parameters and electric properties of the manufactured spiral type resonator are listed in Table 1.

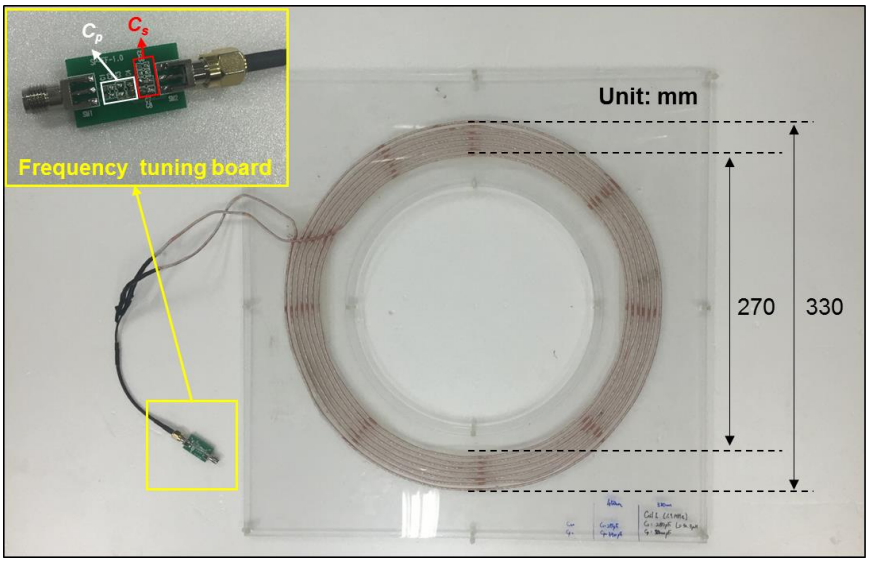

Fig. 4 A spiral type 1.7 MHz resonator with a frequency tuning board

Table 1 Design parameters and electric properties of Tx and Rx resonators

		Tx resonator	Rx resonator
Design parameter	Number of turns	7 turns	
	Inner diameter	270 mm	
	Outer diameter	330 mm	
	Litz wire diameter	2.3 mm	
	Pitch (spacing between wires)	2.3 mm	
	Shunt capacitor (C_p)	5400 pF	3600 pF
	Series capacitor (C_s)	276.8 pF	280 pF
Electric properties	Resonant frequency	1.7 MHz	
	Inductance	30.3 uH	29.7 uH
	Resistance	0.2 Ω	0.2 Ω
	Quality factor (Q)	257.6	252.5

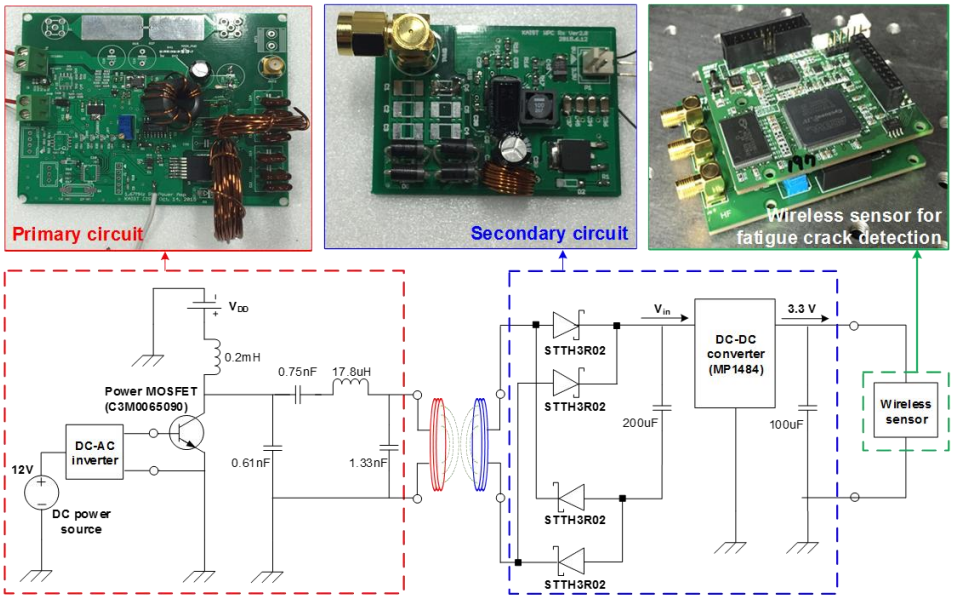

Fig. 5 The primary and secondary circuits connected to Tx and Rx resonators, and a wireless sensor for fatigue crack detection (Liu *et al*. 2014)

Fig. 5 shows the primary and secondary circuits connected to Tx and Rx resonators, and their simplified circuit models. The proposed MR-WPT system is used to power a wireless sensor for fatigue crack detection that was previously developed by the authors' group (Liu *et al.* 2014).

First, a 12 VDC power source is applied to the primary circuit, and inverted into 1.7 MHz AC power through a DC-AC inverter. The inverted AC power is amplified by a Class-E amplifier designed for this study to increase power delivery to the load (wireless sensor). The Class-E

amplifier employs zero-voltage-switching to minimize the power dissipation at the pins of a MOSFET during high frequency operation (Sokal *et al.* 1975, Yang *et al.* 2014, Grebennikov *et al.* 2004). The fabricated Class-E amplifier employs an N-channel power MOSFET, C3M0065090 from Wolfspeed^{TM}. A drain voltage, V_{DD}, of the power MOSFET determines the level of power amplification, and its maximum output power is 120 W at V_{DD} = 100 V. The amplified AC power is used to drive Tx resonator through additional impedance matching network to minimize a reflection component (i.e., S_{11}) at the interface between the primary circuit and Tx resonator.

Tx resonator that is driven by the primary circuit produces alternating magnetic fields, and becomes magnetically coupled with Rx resonator that has the identical resonant frequency at 1.7 MHz. This magnetic coupling induces AC power at Rx resonator. The induced AC power is transferred to a full bridge rectifier composed of four ultrafast recovery diodes, STTH3R02 from STMicroelectronics, and converted into DC power. Subsequently, the voltage of DC power is converted into 3.3 V by a DC-DC converter with the rated current of 3 A, MP1484 from Shenzhen Huafuqin Electronics. The converted DC power at 3.3 V is fed to the wireless sensor for fatigue crack detection, so that it can be operated without battery use.

The detailed description of the wireless sensor for fatigue crack detection is shown in Fig. 6. Fig. 6(a) shows two individual modules consisting of the wireless sensor: (1) a high-speed processor and processing core (HP/PC) module and (2) an excitation and sensing (E/S) module. The wireless sensor utilizes a nonlinear ultrasonic technique to detect fatigue crack (Lim *et al.* 2014, Sohn *et al.* 2014). The wireless senor generates and measures ultrasonic waves using piezo-electric (PZT) transducers attached to a target structure, and a crack is detected by extracting nonlinear ultrasonic modulation components produced by it. The operation of the wireless sensor is divided into two steps as shown in Fig. 6(b). During the step (1), the HP/PC module generates an ultrasonic signal in digital format and transfers it to the E/S module. Then, E/S module converts the signal from digital into analog format, and drives excitation PZT transducers. Structural responses are measured by a sensing PZT transducer in analog format, and sequentially it is converted into digital format to be stored in a data storage. In the step (2), the acquired sensing data is processed using crack detection algorithm embedded in the HP/PC module to determine if there is a fatigue crack or not.

The amount of power and energy consumption for the steps (1) and (2) is 2265.4 mW/ 67.97 J and 634.6 mW/ 139.61 J, respectively. In the current version of the wireless sensor, the main power source is a commercial lithium-ion battery, and energy harvesting options, for example natural light and vibration, can be additionally adopted for charging the battery. However, in this study, the developed MR-WPT system is used to supply power to the wireless sensor instead of a battery, so that this wireless sensor can be ultimately called a battery-less and wireless sensor.

Management of the battery-less and wireless sensor for fatigue crack detection can be briefly summarized as follows. First, the sensor is installed at a fatigue-vulnerable location. Since this sensor does not contain an embedded battery inside, it is basically in a turned-off state. When crack inspection is required, an inspection vehicle with an external power source (i.e., MR-WPT system) approaches to the sensor location, and directly supplies power to turn on the sensor. Then, the sensor starts the inspection process through the steps (1) and (2), and returns to the turned-off state after the inspection finishes. The same procedures are repeated every inspection period, for example once every 3 weeks, and this interval crack inspection can be considered to be a semi-permanent process because potential failure of the wireless sensor caused by battery problems will not exist.

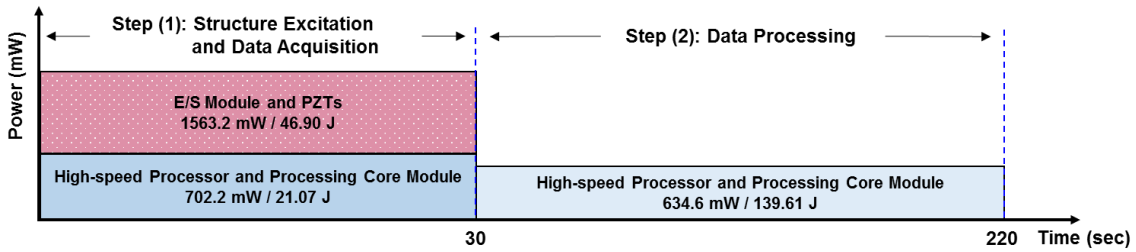

Fig. 6 The wireless sensor for fatigue crack detection (Liu *et al*. 2014): (a) configuration of each module, and (b) amount of power/energy consumption at each operating stage

4. Experimental validation

4.1 Experimental setups

Two concrete specimens are fabricated for the experimental validation of the developed MR-WPT system: (1) a plain concrete and (2) a reinforced concrete. Their sizes and mix proportions are identical, and the only difference is that Φ 15 mm steel rebar with 150-mm spacing at the center is embedded in the reinforced concrete specimen. The mix proportion of the concrete specimens described in Table 2 is similar to the one used for a typical bridge deck. They are casted in rectangular wooden molds of dimensions 600 × 600 × 300 mm^3, and cured for 28 days before testing. Figs. 7(a) and 7(b) respectively show the top and side views of the reinforced concrete specimen fabricated for this study. The distance of the steel rebar from the bottom concrete surface is set to 50 mm, as described in Fig. 7(b).

Figs. 8(a) and 8(b) show the overall configurations of the wireless power transfer experiment through free space and concrete specimens, respectively. S_{11} and S_{21} are measured using a vector network analyzer, ZVH8 from Rodhe & Schwarz GmbH, for 450 mm and 500 mm distances (D) between Tx and Rx resonators. In Fig. 8(b), three layers of concrete blocks (190 × 90 × 57 mm^3) are stacked, and Rx resonator is placed on the top of the third layer. Then, one more layer is stacked again on the top of Rx resonator, and the concrete specimen is placed. Finally, additional layers of concrete blocks and Tx resonator are placed on the top of the concrete specimen. The distance between Rx resonator and the bottom of the concrete specimen is fixed at 60 mm, and the distance between Tx resonator and the top concrete surface is varied from 90 mm to 140 mm. During the experiments, the centers of Tx and Rx resonators are aligned with that of the reinforcement grid and the center of the concrete specimen.

Table 2 Mix proportion for the concrete

	Gravel	Sand	Water	Cement	WRA
Unit weight (kg/m^3)	869	778	164	480	58.9

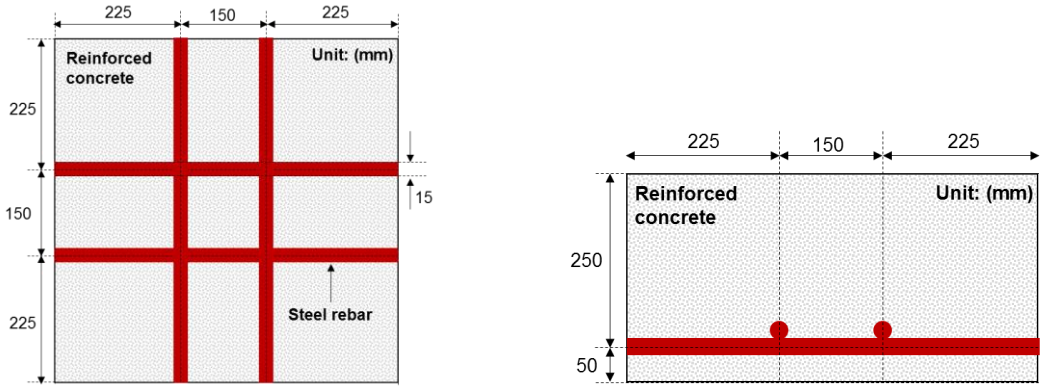

Fig. 7 A 300 mm-thick reinforced concrete specimen with Φ 15 mm steel rebar: (a) a top and (b) side view

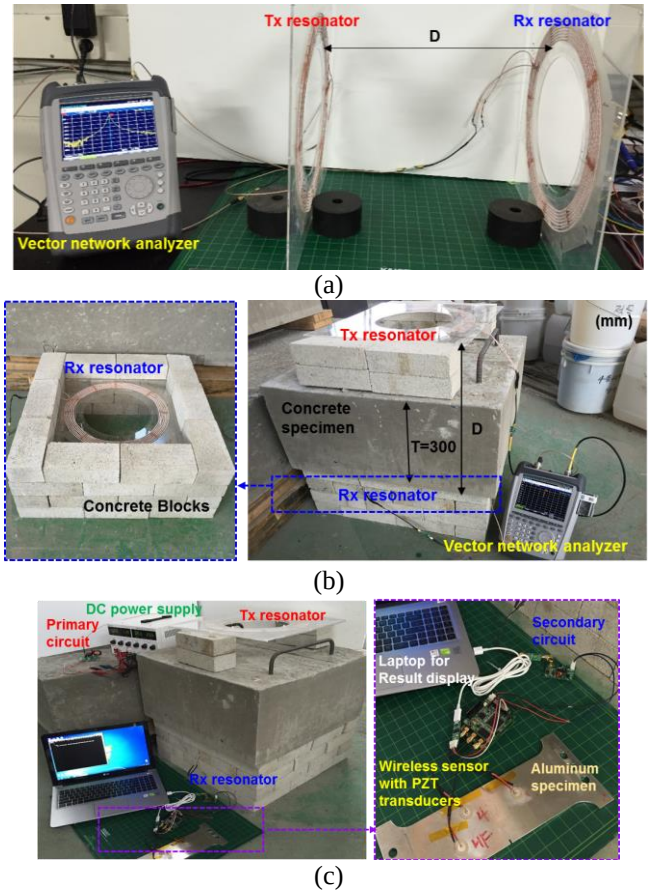

Fig. 8 Experimental setup for performance validation of the developed MR-WPT system: (a) measuring S_{11} and S_{21} through free space and (b) concrete specimen, and (c) operating a wireless sensor for fatigue crack detection

In Fig. 8(c), the primary and the secondary circuits fabricated in this study are connected to Tx and Rx resonators, respectively, and the battery-less and wireless crack sensor is powered by the developed MR-WPT system instead of a solid-state battery. The operating voltage of the wireless sensor is 3.3 V, and its normal and peak power consumptions are 2.0 W and 2.3 W, respectively. The sensor is attached to the aluminum plate (6061 T6) that was previously tested by the authors' group (Liu *et al.* 2014) as described in Fig. 9(a) with its detailed dimensions. A 17 mm-long fatigue crack is produced at an artificial notch in this aluminum plate via cyclic loading test using a universal testing machine (INSTRON 8801). Fig. 9(b) shows a close-up image of the created fatigue crack.

Three PZT transducers (APC International) with 18 mm in diameter and 0.508 mm thick are installed on the aluminum plate: PZT 1 for high frequency (HF) excitation, PZT 2 for low frequency (LF) excitation and PZT 3 for sensing. Each PZT transducer is located 60 mm away from the notch-tip as shown in Fig. 9(a). Those PZT transducers are accordingly connected to the E/S module of the battery-less and wireless sensor. In this experiment, HF is fixed at 197 kHz and LF is swept from 40 kHz to 50 kHz in 1 kHz increments. Then, the magnitudes of the modulation components are computed using on-board processing of the wireless sensor, first powered by a 3.3 V commercial battery and then by the proposed MR-WPT system.

4.2 Experimental results

Figs. 10, 11 and 12 show the measured S_{11} and S_{21} values between Tx and Rx resonators, when power is transferred for distances of 450 mm and 500 mm through free space, plain concrete and reinforced concrete, respectively. Note that, because the magnetic coupling between Tx and Rx resonators varies depending on the transmitting medium and D, the impedances of the primary and secondary circuits are altered for each test setup using the impedance matching board so that the MR-WPT system resonates at its operating frequency, 1.7 MHz. To achieve its optimum performance, S_{11} (i.e., the reflection coefficient) is always kept under -15 dB by matching the impedance of Tx resonator to the input impedance of the vector network analyzer, 50 Ω.

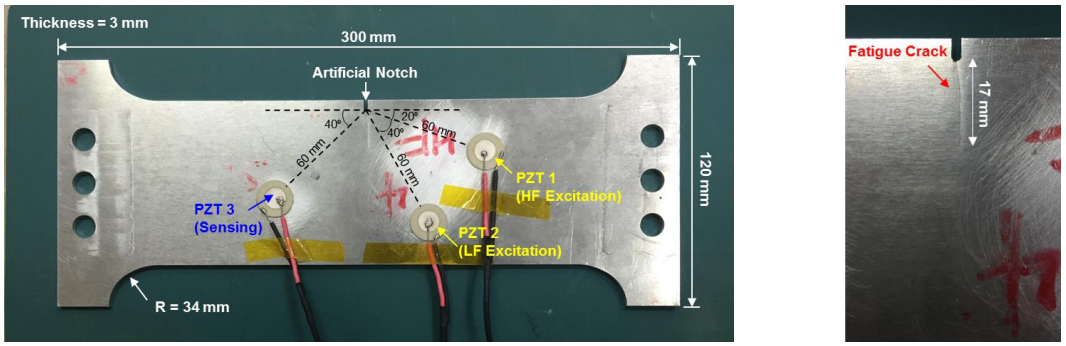

(a) (b)

Fig. 9 (a) Detailed dimensions of the aluminum plate and locations of the PZTs and (b) a close-up image of the created fatigue crack. HF and LF mean high and low frequencies, respectively

PTEs for different test configurations are summarized in Fig. 13. The deterioration of PTE can be attributed to (1) an increase of the transfer distance, (2) EM wave reflections at the concrete specimen surfaces and (3) absorption of EM waves at the steel rebar. Overall, 7.20% of the mean deterioration is observed because of increase of the transfer distance. 300-mm-thick concrete causes an additional 10.17% reduction of PTE, and the steel rebar causes a reduction of only 3.39 %.

Next, the battery-less and wireless crack sensor is powered by the proposed MR-WPT system, and the magnitudes of the nonlinear modulation components are computed on-board. The same experiment is repeated using a 3.3 V commercial battery, and the modulation magnitudes obtained from two different power sources are compared in Fig. 14. The blue bar with the solid line and the yellow bar with dotted line represent modulation magnitudes from a 3.3 V commercial battery and the developed MR-WPT system, respectively. The two tests show almost identical results with differences within normal variations.

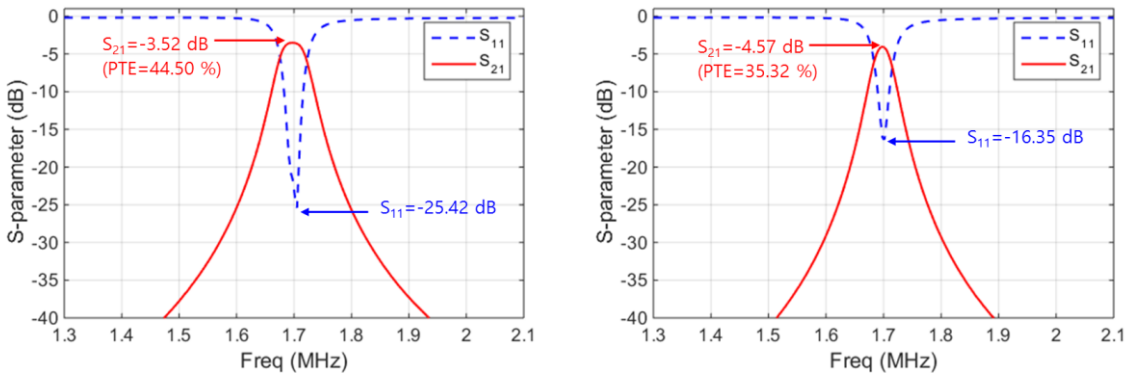

Fig. 10 S_{11} and S_{21} for WPT through free space at (a) D = 450 mm and (b) D = 500 mm

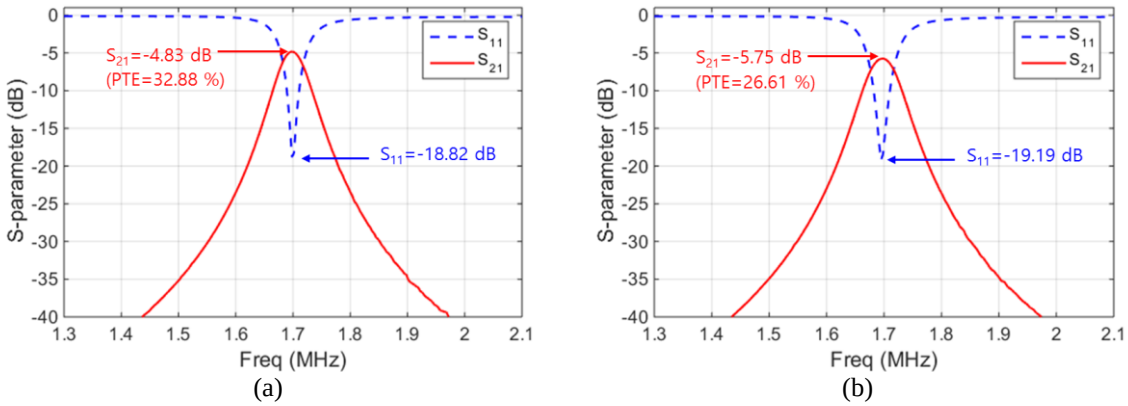

Fig. 11 S_{11} and S_{21} for WPT through the plain concrete at (a) D = 450 mm and (b) D = 500 mm

While PTE only between Tx and Rx resonators is measured in Fig. 13, Table 3 shows PTE of the all system additionally considering (1) power consumption of the electric components in the primary and the secondary circuits, and (2) EM wave reflections because of impedance mismatch between the circuits and the resonators. The transmitted power is measured through reinforced concrete after replacing the wireless sensor with a 5 Ω cement resistor. The input power is 16.27 W and 19.84 W at D = 450 mm and D = 500 mm, respectively, and the received power is 3.43 W. Accordingly, the overall system PTE is measured to be 21.34% at D = 450 mm and 17.29% at D = 500 mm.

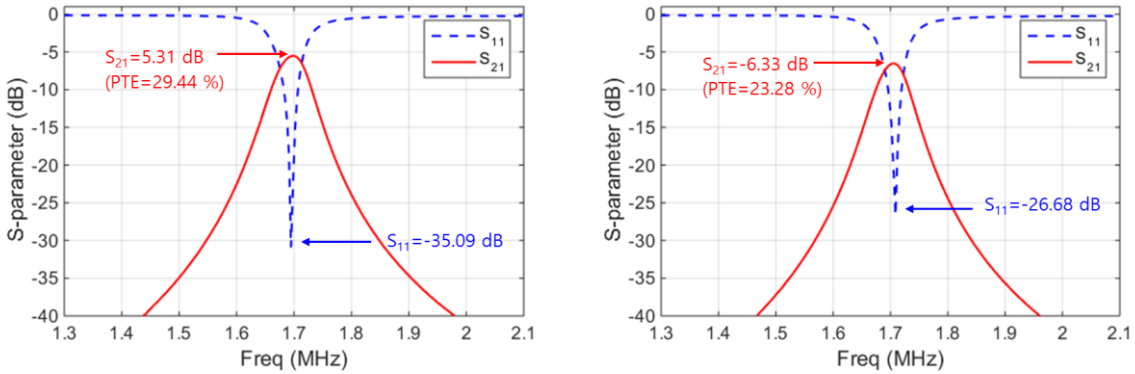

Fig. 12 S_{11} and S_{21} for WPT through the reinforced concrete at (a) D = 450 mm and (b) D = 500 mm

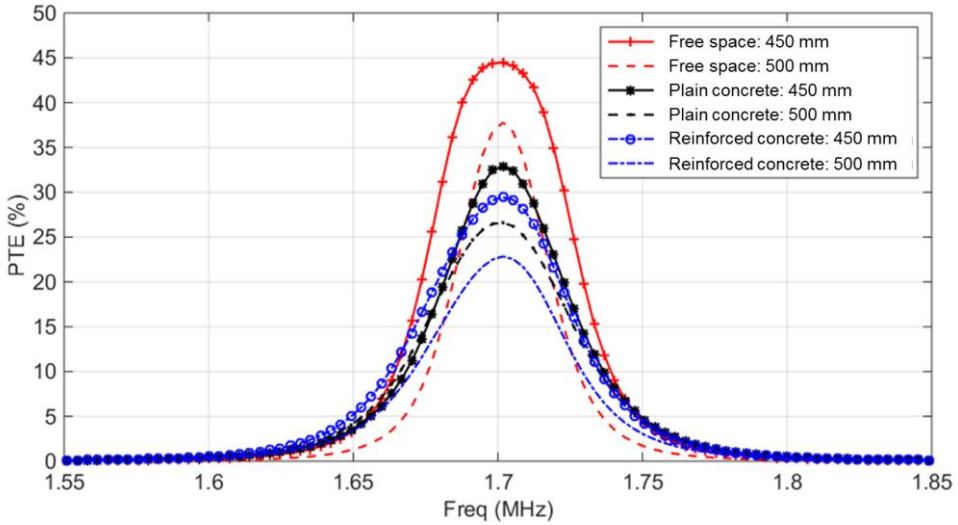

Fig. 13 PTE variations between Tx and Rx resonators through: (1) free space, (2) plain concrete and (3) reinforced concrete

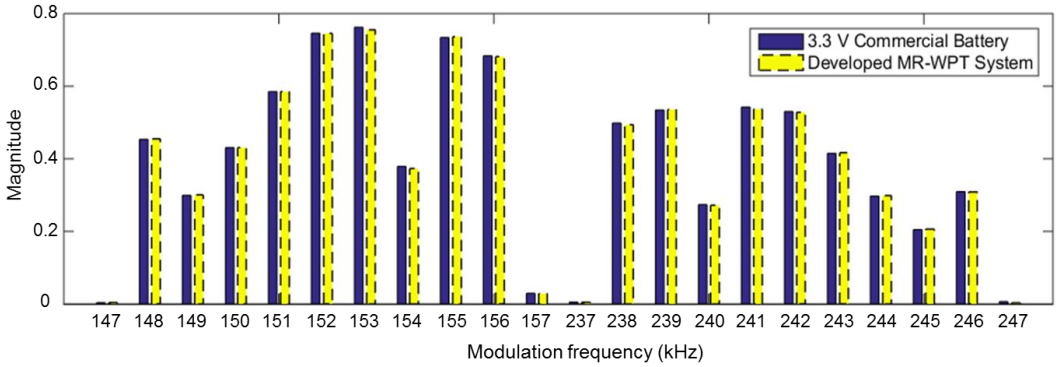

Fig. 14 Comparison of nonlinear modulation components computed by on-board processing of the wireless sensor when the sensor is powered by a 3.3 V commercial battery and the developed MR-WPT system

Table 3 The overall system PTE of the developed MR-WPT system through the reinforced concrete structure at D = 450 mm and D = 500 mm

	D = 450 mm			D = 500 mm		
	Voltage (V)	Current (A)	Power (W)	Voltage (V)	Current (A)	Power (W)
Input	20.6	0.79	16.27	24.5	0.81	19.84
Output	3.3	1.04	3.43	3.3	1.04	3.43
System efficiency (%)	-		*21.34*	-		*17.29*

5. Conclusions

This study proposes and develops a magnetic resonance based wireless power transfer (MR-WPT) system composed of primary and secondary circuits and transmitting and receiving resonators. The developed MR-WPT system enables: (1) the transfer of more than a few Watts of power through a reinforced concrete structure at a mid-range distance of over 500 mm; (2) the operation of a wireless sensor without any embedded energy storage; and (3) the carrying-out of need-based instantaneous wireless power transfer using an external power source. Its performance was validated by evaluating and comparing the power transfer efficiency (PTE) through different transmitting media: (1) free space, (2) plain concrete and (3) reinforced concrete. The overall system PTE through the reinforced concrete was 21.34% at D = 450 mm and 17.29% at D = 500 mm, respectively, with the transferred power of 3.43 W. The existence of concrete and steel rebar degraded PTE by 10.17% and 3.39%, respectively. However, the developed MR-WPT system provided enough power to operate a battery-less and wireless crack sensor previously developed by the authors' group. On-board data processing results measured under two different power feeding conditions, using a commercial battery and the developed MR-WPT system, were practically identical with only a 3.4% mean error. To make the proposed MR-WPT system more attractive for field applications, additional improvements are warranted. First, an adaptive impedance matching circuit and algorithm are necessary to cope with the arbitrary variance of

media impedance. Second, feasibility of the developed MR-WPT system should be tested for real structures. Third, PTE can be improved by optimizing the resonators' design parameters and altering resonator configurations.

Acknowledgments

This study is supported by a grant from Smart Civil Infrastructure Research Program (13SCIPA01) funded by Ministry of Land, Infrastructure and Transport (MOLIT) of Korea government and the Center for Integrated Smart Sensors funded by the Ministry of Science, ICT & Future Planning as Global Frontier Project (CISS- 2015M3A6A6066117).

References

Alippi, C. and Galperti, C. (2008), "An adaptive system for optimal solar energy harvesting in wireless sensor network nodes", *IEEE T. Circuits-I.*, **55**(6), 1742-1750.

Antonini, G., Orlandi, A. and D'Elia, S. (2003), "Shielding effects of reinforced concrete structures to electromagnetic fields due to GSM and UMTS systems", *IEEE T. Magn.*, **39**(3), 1582-1585.

Beh, T.C., Kato, M., Imura, T., Oh, S. and Hori, Y. (2013), "Automated impedance matching system for robust wireless power transfer via magnetic resonance coupling", *IEEE T. Ind. Electron.*, **60**(9), 3689-3698.

Cho, S., Jo, H., Jang, S., Park, J., Jung, H.J., Yun C.B., Spencer, B.F. and Seo, J.W. (2010), "Structural Health Monitoring of a Cable-stayed Bridge using Wireless Smart Sensor Technology: data analysis", *Smart. Struct. Syst.*, **6**(5-6), 461-480.

Dai, J. and Ludois, D.C. (2015), "A survey of wireless power transfer and a critical comparison of inductive and capacitive coupling for small gap applications", *IEEE T. Power Electr.*, **30**(11), 6017-6029.

Farhey, D.N. (2005), "Bridge instrumentation and monitoring for structural diagnostics", *Struct. Health. Monit.*, **4**(4), 301-318.

Grebennikov, A. (2004), *Load Network Design Techniques for Class E RF and Microwave Amplifiers*, High Frequency Electronics, July.

Hao, S. (2010), "I-35W bridge collapse", *J. Bridge. Eng.*, **15**(5), 608-614.

Hu, X. and Wang, B. (2013), "A wireless sensor network-based structural health monitoring system for highway bridges", *Comput - Aided. Civ. Inf.*, **28**, 193-209.

Imura, T. and Hori, Y. (2011), "Maximizing air gap and efficiency of magnetic resonant coupling for wireless power transfer using equivalent circuit and neumann formula", *IEEE T. Ind. Electron.*, **58**(10), 4746-4752.

Jang, S., Jo, H., Cho, S., Mechitov, K., Rice J.A., Sim S.H., Jung H.J., Yun, C.B., Spencer, B.F. and Seo, J.W. (2010), "Structural health monitoring of a cable-stayed bridge using wireless smart sensor technology: deployment and evaluation", *Smart. Struct. Syst.*, **6**(5-6), 439-459.

Jonah, O. and Georgakopoulos, S.V. (2013) "Wireless power transfer in concrete via strongly coupled magnetic resonance", *IEEE T. Antenn. Propag.*, **61**(3), 1378-1384.

Jung, H.J., Park, J. and Kim, I.H. (2011), "An energy harvesting system using wind-induced vibration of a stay cable for powering a wireless sensor node", *Smart Mater. Struct.*, **20**(7), 1-9.

Kurs, A., Karalis, A., Moffatt, R., Joannopoulos, J.D., Fisher, P. and Soljacic, M. (2007), "Wireless power transfer via strongly coupled magnetic resonances", *Science*, **317**(5834), 83-86.

Li, J., Hao, H., Fan, K. and Brownjohn, J. (2015), "Development and application of a relative displacement sensor for structural health monitoring of composite bridges", *Struct. Control Health Monit.*, **22**, 726-742.

Lim, H.J., Sohn, H., DeSimio, M.P. and Brown, K. (2014), "Reference-free fatigue crack detection using

nonlinear ultrasonic modulation under changing temperature and loading conditions", *Mech. Syst. Signal Pr.*, **45**(2), 468-478.
Liu, P., Yang, S.Y., Lim, H.J., Park, H.C., Ko, I.C. and Sohn, H. (2014), "Development of a wireless nonlinear wave modulation spectroscopy (NWMS) sensor node for fatigue crack detection", *Proceedings of SPIE International Symposia, Smart Structures & Materials and Nondestructive Evaluation for Health Monitoring and Diagnostics*, San Diego, CA, March.
Lopez-Higuera, J.M., Cobo, L.R., Incera, A.Q. and Cobo, A. (2011), "Fiber optic sensors in structural health monitoring", *J. Lightwave Technol.*, **29**(4), 587-608.
Lynch, J.P. and Loh, K.J. (2006), "A Summary Review of Wireless Sensors and Sensor Networks for Structural Health Monitoring", *Shock Vib. Digest*, **38**(2), 91-128.
Lynch, J.P., Wang, Y., Loh, K.J., Yi, J.H. and Yun, C.B. (2006), "Performance monitoring of the geumdang bridge using a dense network of high-resolution wireless sensors", *Smart Mater. Struct.*, **15**, 1561-1575.
Moon, S.C., Kim, B.C., Cho, S.Y., Ahn, C.H. and Moon, G.W. (2014), "Analysis and design of a wireless power transfer system with an intermediate coil for high efficiency", *IEEE T. Ind. Electron.*, **61**(11), 5861-5870.
Nguyen, T., Chan, T.H.T., Thambiratnam, D.P. and King, L. (2015), "Development of a cost-effective and flexible vibration DAQ system for long-term continuous structural health monitoring", *Mech. Syst. Signal Pr.*, **64-65**, 313-324..
Ogunsola, A., Reggiani, U. and Sandrolini, L. (2006), "Modelling shielding properties of concrete", *Proceedings of the 17th International Zurich Symposium on Electromagnetic Compatibility*, Singapore, February.
Park, H.J., Sohn, H., Yun, C.B., Chung, J. and Kwon, I.B. (2010), "A wireless guided wave excitation technique based on laser and optoelectronics", *Smart. Struct. Syst.*, **6**(5), 749-765.
Raghavan A. and Cesnik, C.E.S. (2007), "Review of guided-wave structural health monitoring", *Shock Vib. Digest*, **39**(2), 91-114.
Richalot, E., Bonilla, M., Wong, M.F., Fouad-Hanna, V., Baudrand, H. and Wiart, J. (2003), "Electromagnetic propagation into reinforced concrete walls", *IEEE T. Microw Theory*, **48**(3), 357-366.
Roh, J.S., Chi, Y.S. and Kang, T.J. (2008), "Electromagnetic shielding effectiveness of multifunctional metal composite fabrics", *Text. Res. J.*, **78**(9), 825-835.
Sample, A.P., Meyer, D.A. and Smit. J.R. (2011) "Analysis, experimental results, and range adaptation of magnetically coupled resonators for wireless power transfer", *IEEE T. Ind. Electron.*, **58**(2), 544-554.
Schallhorn, C. and Rahmatalla, S. (2015), "Crack detection and health monitoring of highway steel-girder bridges", *Struct. Health Monit.*, **14**(3), 281-299.
Sohn, H., Farrar C.R., Hemez, F.M., Shunk, D.D., Stinemates D.W., Nadler, B.R. and Czarnecki, J.J. (2004), *A Review of Structural Health Monitoring Literature: 1996-2001*, Los Alamos National Laboratory Report, February.
Sohn, H., Lim, H.J., Desimio, M.P., Brown, K. and Derriso, M. (2014), "Nonlinear ultrasonic wave modulation for online fatigue crack detection", *J. Sound. Vib.*, **333**(5), 1473-1484.
Sokal, N.O. and Sokal, A.D. (1975), "Class E – a new class of high-efficiency tuned single-ended switching power amplifiers", *IEEE J. Solid-St. Circ.*, **10**(3), 168-176.
Tan, Y.K. and Panda, S.K. (2011), "Energy harvesting from hybrid indoor ambient light and thermal energy sources for enhanced performance of wireless sensor nodes", *IEEE T. Ind. Electron.*, **58**(9), 4424-4435.
Visser, H.J and Vullers R.J.M. (2013), "RF energy harvesting and transport for wireless sensor network applications: Principles and requirements", *P. IEEE*, **101**(6), 1410-1423.
Wei, X., Wang, Z. and Dai, H. (2014), "A critical review of wireless power transfer via strongly coupled magnetic resonances", *Energies*, **7**, 4316-4341.
Yang, J.R., Kim, J. and Park, Y.J. (2014), "Class E power amplifiers using high-Q inductors for loosely coupled wireless power transfer system", *J. Electr. Eng. Technol.*, **9**(2), 569-575.